Probing the Inner Jet of the Quasar PKS 1510−089 with Multi-waveband Monitoring during Strong Gamma-ray Activity

Alan P. Marscher[1], Svetlana G. Jorstad[1,2], Valeri M. Larionov[2,3], Margo F. Aller[4], Hugh D. Aller[4], Anne Lähteenmäki[5], Iván Agudo [6], Paul S. Smith[7], Mark Gurwell[8], Vladimir A. Hagen-Thorn[2,3], Tatiana S. Konstantinova[2], Elena G. Larionova[2], Liudmila V. Larionova[2], Daria A. Melnichuk[2], Dmitry A. Blinov[2], Evgenia N. Kopatskaya[2], Ivan S.Troitsky[2], Merja Tornikoski[5], Talvikki Hovatta[5], Gary D. Schmidt [7], Francesca D. D'Arcangelo[1,9], Dipesh Bhattarai[1], Brian Taylor[1,10], Alice R. Olmstead[1], Emily Manne-Nicholas[1], Mar Roca-Sogorb[6], José L. Gómez [6], Ian M. McHardy[11], Omar Kurtanidze[12], Maria G. Nikolashvili[12], Givi N. Kimeridze[12], and Lorand A. Sigua[12]

marscher@bu.edu

ABSTRACT

We present results from monitoring the multi-waveband flux, linear polarization, and parsec-scale structure of the quasar PKS 1510−089, concentrating on

[1]Institute for Astrophysical Research, Boston University, 725 Commonwealth Avenue, Boston, MA 02215

[2]Astronomical Institute, St. Petersburg State University, Universitetskij Pr. 28, Petrodvorets, 198504 St. Petersburg, Russia

[3]Isaac Newton Institute of Chile, St. Petersburg Branch, St. Petersburg, Russia

[4]Astronomy Department, University of Michigan, 830 Dennison, 500 Church St., Ann Arbor, Michigan 48109-1042

[5]Metsähovi Radio Observatory, Helsinki University of Technology TKK, Metsähovintie 114, FIN-02540 Kylmälä, Finland

[6]Instituto de Astrofísica de Andalucía, CSIC, Apartado 3004, 18080, Granada, Spain

[7]Steward Observatory, University of Arizona, Tucson, AZ 85721-0065

[8]Harvard-Smithsonian Center for Astrophysics, 60 Garden St., Cambridge, MA 02138

[9]Current address: MIT Lincoln Laboratory, 244 WoodSt., Lexington, MA, 02421

[10]Lowell Observatory, Flagstaff, AZ 86001

[11]Department of Physics and Astronomy, University of Southampton, Southampton, SO17 1BJ, United Kingdom

[12]Abastumani Astrophysical Observatory, Mt. Kanobili, Abastumani, Georgia

eight major γ-ray flares that occurred during the interval 2009.0-2009.5. The γ-ray peaks were essentially simultaneous with maxima at optical wavelengths, although the flux ratio of the two wavebands varied by an order of magnitude. The optical polarization vector rotated by 720° during a 5-day period encompassing six of these flares. This culminated in a very bright, $\sim$ 1 day, optical and γ-ray flare as a bright knot of emission passed through the highest-intensity, stationary feature (the "core") seen in 43 GHz Very Long Baseline Array images. The knot continued to propagate down the jet at an apparent speed of $22c$ and emit strongly at γ-ray energies as a months-long X-ray/radio outburst intensified. We interpret these events as the result of the knot following a spiral path through a mainly toroidal magnetic field pattern in the acceleration and collimation zone of the jet, after which it passes through a standing shock in the 43 GHz core and then continues downstream. In this picture, the rapid γ-ray flares result from scattering of infrared seed photons from a relatively slow sheath of the jet as well as from optical synchrotron radiation in the faster spine. The 2006-2009.7 radio and X-ray flux variations are correlated at very high significance; we conclude that the X-rays are mainly from inverse Compton scattering of infrared seed photons by 20-40 MeV electrons.

Subject headings: quasars: individual (PKS 1510−089) — polarization— gamma rays: general — radio continuum: galaxies — X-rays: galaxies

1. Introduction

Attempts to understand relativistic jets of blazars have been greatly advanced by the availability of instruments such as the Very Long Baseline Array (VLBA), the *Rossi* X-ray Timing Explorer (RXTE), and, most recently, the *Fermi* Gamma-ray Space Telescope, together with more traditional telescopes. Long-term multi-waveband monitoring of a number of blazars with these facilities is now providing valuable insights into the physical processes in the jets (e.g., Marscher et al. 2008; Chatterjee et al. 2008; Larionov et al. 2008). This paper presents a rich set of observations of the γ-ray bright quasar PKS 1510−089 ($z = 0.361$), whose jet exhibits apparent motions of emission features that are among the fastest (as high as $45c$) of all blazars observed thus far (Jorstad et al. 2005). We analyze motions of features in the parsec-scale radio jet alongside variability of the optical polarization and flux from radio through γ-ray frequencies. The relative timing of correlated variations probes the structure and physics of the innermost jet regions where the flow is accelerated and collimated, and where the emitting electrons are energized.

2. Observations and Data Analysis

Our observations include imaging with the VLBA at 43 GHz in both total and linearly polarized intensity, with angular resolution near 0.10 milliarcseconds (mas), or a projected distance of 0.50 pc (for $H_\circ = 71$ km s^{-1} Mpc^{-1} and the concordance cosmology; Spergel et al. 2007). We processed the data and created images in a manner identical to that described by Jorstad et al. (2005).

We derived 0.1-200 GeV γ-ray fluxes by analyzing data from the Large Area Telescope (LAT) of the *Fermi* Gamma-ray Space Telescope with the standard software (Atwood et al. 2009). Photon counts from a circular region of radius 20° centered on PKS 1510−089 were fit by single power-law spectral models of this source, PKS 1502+106, and PKS 1508−055, plus model v02 of the Galactic and extragalactic backgrounds. The mean slope of the photon spectrum for 2009.0-2009.5 for 7-day integrations, -2.48 ± 0.05, matched that reported by Abdo et al. (2009) for 2008.6-2008.83. Our final fluxes are from 1-day integrations using this slope, with a detection criterion that the maximum-likelihood test statistic (Mattox et al. 1996) exceed 9.0.

We obtained 2.4-10 keV X-ray fluxes with the RXTE PCA. We processed the data as described by Marscher et al. (2008), fitting the photon count spectrum with a single power law plus photoelectric absorption corresponding to a neutral hydrogen column density of 8×10^{20} cm^{-2}. In addition, we measured flux densities at: 14.5 GHz with the 26 m antenna of the University of Michigan Radio Astronomy Observatory (see Aller et al. 1985); 37 GHz with the 14 m telescope of the Metsähovi Radio Observatory (see Teräsranta et al. 1998); and frequencies near 230 GHz with the Submillimeter Array (see Gurwell et al. 2007).

We measured the degree of optical linear polarization P and its position angle χ with: the 0.4 m telescope of St. Petersburg State University; the 0.7 m telescope at the Crimean Astrophysical Observatory; the PRISM camera on the Lowell Observatory 1.83 m Perkins Telescope; the Steward Observatory 2.3 and 1.54 m telescopes [1]; and the 2.2 m telescope at Calar Alto Observatory, under the MAPCAT program. The data analysis procedures for the various telescopes are described in D'Arcangelo et al. (2007); Larionov et al. (2008); Jorstad et al. (2010). We also obtained optical (R-band) flux densities from photometric observations at the six telescopes listed above, the 2.0 m Liverpool Telescope, and the 0.7 m Meniscus Telescope of Abastumani Astrophysical Observatory. We have added data from Yale University [2].

[1]Data listing: http://james.as.arizona.edu/∼psmith/Fermi

[2]Data listing: http://www.astro.yale.edu/smarts/glast

3. Observational Results and Discussion

A number of flares are apparent in the 2008-09 radio to γ-ray light curves (Fig. 1, which includes γ-ray data from AGILE in 2008 March; D'Ammando et al. 2009). Of particular interest is the first half of 2009 (Fig. 2), during which eight major γ-ray flares are apparent. The VLBA images (Fig. 3) feature a bright "core," presumed stationary, from which knots of emission separate at apparent superluminal speeds. We detect two new knots, with apparent speeds of $24 \pm 2\,c$ and $21.6 \pm 0.6\,c$. The first passed the core on JD 2454675 ± 20, as the X-ray flux reached a sharp peak, and ~ 2 weeks after a broad maximum in the 14.5 GHz flux (see Fig. 1). The second knot passed the core on JD 2454959 ± 4, essentially simultaneous with the extremely sharp, high-amplitude optical/γ-ray flare 8 on JD 2454962 (Fig. 2). We argue below that this knot was responsible for flares 3-8 and possibly 1-2.

Flare 8 coincides with the end of a 50-day rotation of χ by 720° that started near flare 3 (see Fig. 4). This striking phenomenon can be explained either by a stochastic process or by a coherent magnetic field geometry of the flaring region. In the stochastic interpretation, the magnetic field is turbulent (see Jones 1988; Marscher et al. 1992; D'Arcangelo 2009) and the apparent rotation results from a random walk of the resultant polarization vector direction as cells with random magnetic field orientations enter and then exit the emission region. According to our simulations (described by D'Arcangelo et al. 2007), one rotation by $> 720°$ similar to that of PKS 1510−089 and lasting 50 ± 10 days occurs once per $\sim 2,000$ days. The probability that such a random apparent rotation would coincide so closely with a specific 50-day period of elevated γ-ray flux is extremely small, $\sim 0.1\%$. Furthermore, the model predicts equally probable clockwise and counterclockwise rotations of χ in the same object, while the $\sim 180°$ rotation of χ between JD 2454990 and 2455000 (see Fig. 4) proceeded at the same counterclockwise rate as during the final stage of the larger rotation. This implies that the rotation is dictated by geometry, with the accompanying minor flare occurring in the same location as flare 8.

We observed a similar, but shorter, rotation of the optical polarization in BL Lac in 2005 (Marscher et al. 2008). We apply our phenomenological model developed to explain that event to PKS 1510−089. A moving emission feature follows a spiral path as it propagates through the toroidal magnetic field of the acceleration and collimation zone of the jet (Komissarov et al. 2007). The spiral motion is caused either by rotation of the flow (Vlahakis 2006) or a helical stream of electron-positron pairs injected from the black hole's ergosphere (Williams 2004). The secular increase in the rate of rotation (see Fig. 4) is due to an increasing Doppler factor as the flow accelerates until it reaches the core, since the Lorentz factor increases as the cross-sectional radius of the jet (Vlahakis & Königl 2004; Vlahakis 2006; Komissarov et al. 2007). [However, the rest-frame angular velocity of the emission feature

cannot decrease to conserve specific angular momentum as the jet expands (Steffen et al. 1995; Vlahakis 2006), hence the spiral path followed by the centroid of the feature must maintain a constant radius of helical motion to avoid this.] The emission feature must cover most of the cross-section of the jet in order to create substantial flares and to cancel most of the polarization (from different orientations of the toroidal magnetic field across the feature) while leaving a residual of $\lesssim 10\%$, with χ rotating systematically as the feature proceeds down the jet. Front-to-back light-travel time delays also cancel some polarization by stretching the feature along the spiral path as viewed by the observer. Synchrotron flares occur when the energization of electrons increases suddenly over some or all of the emission region; our model does not attempt to explain these sudden surges in particle acceleration. The solid curve in the bottom panel of Figure 4 shows the fit to the variation of χ of the model, with parameter values that are typical but probably not unique. The bulk Lorentz factor increases linearly with longitudinal distance down the jet from a value of 8 at the onset of the rotation to 24 at the end. The viewing angle of the jet axis is 1.4° in the model, so the Doppler factor increases from 15 to 38 during this time, and the final apparent speed is $21c$, matching the observed value within the uncertainties. The inflections of the curve are due to changing aberration, which we calculate with the equations of Königl & Choudhuri (1985). The scenario proposed in that paper, in which the jet twists from helical instabilities, can explain the rotation of χ but not the observed low, randomly changing degree of polarization. The secular increase both in the rate of rotation of χ and in optical flux during the first half of the outburst results from the acceleration of the flow and consequent enhanced beaming.

Flare 8, featuring the highest optical flux observed since 1948 (Liller & Liller 1975), occurred as the rotation of χ was ending and the new superluminal knot was passing the core. This event can be explained by compression of the knot by a standing conical shock (Marscher et al. 2008). According to our model, when the knot passed the core it was propagating down the jet at 0.3 pc day^{-1} in our frame, and had traveled 17 pc downstream since the rotation of χ began. The transverse radius of the jet at this point is $\sim 2 \times 10^{17}$ cm, based on the opening angle of the jet $\sim 0.2°$ derived by Jorstad et al. (2005). The propagation rate, plus the 1-day timescale of the flare, sets the longitudinal size of the optical flare region at ~ 0.3 pc. We associate this size with the distance moved by an electron radiating at R-band before it loses too much energy to continue doing so. To determine the energy loss rate for all of the events, we first calculate the ratio of γ-ray (> 100 MeV) to synchrotron luminosity (which equals the ratio of inverse-Compton to synchrotron loss rate), $\zeta_{\rm gs}$, of the peak of flares 1-8 to be 70, 30, 40, 40, 30, 10, 40, and 9, respectively. We estimate the luminosity of the synchrotron radiation, whose spectral energy distribution peaks at infrared wavelengths, as the R-band flux density multiplied by $\nu_R = 4.7 \times 10^{14}$ Hz, by 1.27 to correct for extinction (Schlegel et al. 1998), and then by

6 to convert roughly to bolometric luminosity (see Kataoka et al. 2008). We then derive that the magnetic field $B \sim [(6 \times 10^6 \text{ s})(\Gamma/20)c/(0.3\xi \text{ pc})]^{2/3}(\delta/40)^{1/3} \sim 0.4\xi^{-2/3}$ G during flare 8, where $\xi \equiv (u_\mathrm{B} + u_\mathrm{phot})/u_\mathrm{B}$, $\xi\zeta_\mathrm{gs} \sim 9$ if the seed photons originate from outside the emission feature, $\xi \sim 1$ for mainly first-order SSC, and $\xi \sim \zeta_\mathrm{gs}^{1/2} \sim 3$ for combined first- and second-order SSC. We therefore obtain $B \sim 0.1$–0.4 G, with the highest value for the first-order SSC case. The (toroidal) magnetic field at the start of the rotation of χ was then ~ 1 G.

The 50-day rotation of χ implies that a single moving emission feature was responsible for the entire outburst encompassing flares 3-8. We identify this feature as the superluminal knot seen later in the VLBA images (Fig. 3), whose polarization vector lies in the same direction as in the optical shortly after flare 8. Our observations therefore demonstrate that the high-energy emission from the jet of PKS 1510−089 is quite complex, arising from different regions and probably by multiple emission mechanisms as a *single disturbance* propagates down the jet. Both the γ-ray and optical emission is highly variable, but not always in unison. This is unexpected, since when $B \sim 0.1$–1 G, electrons with the same energies, $\gamma_e \sim 10^{3.5\pm0.3}$ in rest-mass units, should be involved in optical synchrotron radiation and inverse Compton scattering of optical or IR photons to γ-ray energies.

When the emission feature was close to the base of the jet, electrons in the jet could have scattered the broad emission-line region or accretion-disk photons to γ-ray energies as the disturbance first became optically thin to photon-photon pair production (see, e.g., Ghisellini & Tavecchio 2009; Dermer et al. 2009). We speculate that this could correspond to flares 1-2. In this case, the subsequent quiescent period would imply that there is a section of the jet where neither seed photons nor electrons with $\gamma_e \gtrsim 10^3$ are abundant.

We conclude that some or all of γ-ray flares 1-4 and 7, with very weak optical counterparts, were caused by sudden increases in the local seed photon field at optical or IR wavelengths rather than by increased energization of electrons. The time scales of variability limit the size of each source of seed photons to $a \lesssim 1$ pc—not much larger than the cross-sectional radius of the jet, ~ 0.1 pc—while the luminosity of each would need to be $\sim 3 \times 10^{43}(\zeta_\mathrm{gs}/60)(\Gamma/20)^{-2}(B/0.4 \text{ G})^2(a/0.1 \text{ pc})^2 \text{erg s}^{-1}$ if the source lies at the periphery of the jet, and higher if more remote. This luminosity is too high for any commonly occurring cosmic object located parsecs from the central engine, but could be obtained in a relatively slow sheath surrounding the ultra-fast spine of the jet responsible for the high superluminal motion (Ghisellini et al. 2005). Moving knots or standing shocks in the sheath could produce the requisite number of seed photons while being too poorly beamed to contribute substantially to the observed flux. The relatively slow motion and gradual evolution of such features implies that they should persist for years, in which case another series of flares in the near

future should exhibit a similar pattern of variability and appearance of a superluminal knot.

Flares 5 and 8 included rapid optical flaring that required sudden energization of electrons to $\gamma \sim 10^{3.5\pm0.3}$. This suggests that the flaring γ-rays could have been created by the SSC process, an inference that is supported by the lower value of $\zeta_{\rm gs}$ than for the other flares. This ratio was, however, much greater than unity, which implies that second-order scattering contributed significantly to the γ-ray flux (e.g., Bloom & Marscher 1996). We should therefore expect a different slope of the γ-ray photon spectrum for these flares than for flares 1-4 and 7. There are a sufficient number of photon counts to measure the slopes for flares 5, 7, and 8: -2.36 ± 0.09, -2.73 ± 0.17, and -1.92 ± 0.21, respectively. The probability that these are the same is $\sim 0.2\%$. Detailed modeling is needed to determine the slopes expected for the different radiation mechanisms.

The extremely high optical flux and polarization of flare 8 imply that the magnetic field was higher and more ordered for this event than for other flares. This is consistent with our interpretation that the 43 GHz core—where flare 8 occurred—is a standing shock. The low value of $\zeta_{\rm gs}$ implies that the magnetic field was compressed by a factor ~ 2 over the previous flare. We suggest that the emission region responsible for flare 5, when the polarization increased to $> 20\%$, was a subset of the entire disturbance, so that there was less cancellation of the polarization. This indicates that the flare was caused by unusually efficient energization of electrons over only part of the disturbance, although we have insufficient information to determine the cause. In contrast, flares 6 and 7 occurred when the polarization was quite low, which implies that electrons were accelerated less intensely throughout the entire disturbance.

The flare in 2008 September (JD 2454700-2454750; Fig. 1) is of a different nature than flares 1-8. It took place one month after a very bright superluminal knot passed through the core (which coincided with the peak of a major X-ray flare), consistent with the finding of Jorstad et al. (2001) and Lähteenmäki & Valtaoja (2003) that high γ-ray states often follow the time when a new superluminal knot coincides with the core or a millimeter-wave outburst starts. The frequency-dependent delays — the emission peaked first at optical, then γ-ray (10-day lag), and then radio and X-ray (24-day lag) frequencies — contrast with the simultaneity of the optical and γ-ray maxima of flares 2, 5, 7, and 8. The time delays imply that a power law is maintained over only a limited range of electron energies, with the range changing as a knot separates from the core.

Since 1996, the X-ray emission has correlated better with the 14.5 GHz variations than with those at higher frequencies (Marscher 2006). During the 2006-2009 period covered by Figure 5, the correlation is significant at $> 99\%$ confidence. The electrons radiating at 14.5 GHz near the core have energies $\gamma_e \sim$ 20-40 in rest mass units, far too small to

scatter the 14.5 GHz photons to X-ray energies. For this reason, we conclude, as have Kataoka et al. (2008), that these electrons produce the X-rays via inverse Compton scattering of IR seed photons from either the sheath of the jet or a source outside the jet, such as a dust torus (Błażejowski et al. 2000). In this case, the X-ray variability is in response to both the evolution of the electron energy distribution—which affects the radio emission in a similar way — and changes in the seed photon density as a knot propagates down the jet. In the observer's frame, the radiative energy loss time scale of $\gamma_e \sim 30$ electrons, $t_{\rm loss} \sim 3 \times 10^7 B^{-2} \zeta_{\rm gs}^{-1} \delta^{-1}$ s, ~ 5 days when $B \sim 0.4$ G and $\delta\zeta_{\rm gs} \sim 400$. This is commensurate with the fastest X-ray and radio variability that we have observed.

4. Conclusions

Our comprehensive dataset has revealed some patterns that allow us to probe the locations and causes of the high-energy emission in PKS 1510−089. The rotation of the optical polarization vector over 50 days in 2009, as multiple γ-ray and optical flares took place, implies that a single emission feature—the superluminal knot later seen in our VLBA images—was responsible for these variations. As for BL Lac (Marscher et al. 2008), we model this as a structure that followed a spiral path through a helical magnetic field where the jet flow accelerates. The γ-ray to synchrotron flux ratio varied greatly among the different flares. This requires local sources of seed photons from both within the jet and just outside, probably in a surrounding sheath. As a consequence, flares erupt at a variety of locations as disturbances pass down the jet. Future comprehensive multi-waveband monitoring plus VLBA imaging will determine the extent to which our findings apply to the general population of blazars.

Funding of this research included NASA grants NNX08AJ64G and NNX08AV65G and NNX08AV65G, NSF grants AST-0907893 and AST-0607523 (U. Michigan), Russian RFBR grant 09-02-0092, Spanish "Ministerio de Ciencia e Innovación" grant AYA2007-67626-C03-03, the Academy of Finland, the University of Michigan, and Georgian National Science Foundation grant GNSF/ST08/4-404. The VLBA is an instrument of the National Radio Astronomy Observatory, a facility of the NSF, operated under cooperative agreement by Associated Universities, Inc. The Calar Alto Observatory is jointly operated by the Max-Planck-Institut für Astronomie and the Instituto de Astrofísica de Andalucía-CSIC. The SMA is a joint project between the Smithsonian Astrophysical Observatory and the Academia Sinica Institute of Astronomy and Astrophysics, funded by the Smithsonian Institution and the Academia Sinica. The Liverpool Telescope, operated on the island of La Palma by Liverpool John Moores University in the Spanish Observatorio del Roque de los Muchachos of the Instituto de Astrofisica de Canarias, is funded by the UK Science and

Technology Facilities Council.

Facilities: VLBA, RXTE, Fermi, Liverpool:2m, Perkins, Steward:2.3m,1.54m, Calar Alto:2.2m, UMRAO, SMA

REFERENCES

Abdo, A., et al. 2009, ApJS, 183, 46

Aller, H. D., et al. 1985, ApJS, 59, 513

Atwood, W. B., et al. 2009, ApJ, 697, 1071

Błażejowski, et al. 2000, ApJ, 545, 107

Bloom, S. D., & Marscher, A. P. 1996, ApJ, 461, 657

Chatterjee, R., et al. 2008, ApJ, 689, 79

D'Ammando, F. 2009, A&A, 508, 181

D'Arcangelo, F. D., et al. 2007, ApJ, 659, L107

D'Arcangelo, F. D. 2009, Ph.D. Thesis, Boston University

Dermer, C. D., Finke, J. D., Krug, H., & Böttcher, M. 2009, ApJ, 692, 32

Ghisellini, G., & Tavecchio, F. 2009, MNRAS, 397, 985

Ghisellini, G., Tavecchio, F., & Chiaberge, M. 2005, A&A, 432, 401

Gurwell, M. A., Peck, A. B., Hostler, S. R., Darrah, M. R., & Katz, C. A. 2007, in From Z-Machines to ALMA: (Sub)millimeter Spectroscopy of Galaxies, ed. A. J. Baker et al., ASP Conf. Ser., 375, 234

Jones, T. W. 1988, ApJ, 332, 678

Jorstad, S. G., et al. 2001, ApJ, 556, 738

Jorstad, S. G., et al. 2005, AJ, 130, 1418

Jorstad, S. G., et al. 2007, AJ, 134, 799

Jorstad, S. G., et al. 2010, ApJ, submitted

Kataoka, J., et al. 2008, ApJ, 672, 787

Komissarov, S. S., Barkov, M. V., Vlahakis, N., & Königl, A. 2007, MNRAS, 380, 51

Königl, A., & Choudhuri, A. R. 1985, ApJ, 289, 188

Lätheenmäki, A., & Valtaoja, E. 2003, ApJ, 580,85

Larionov, V. M., et al. 2008, A&A, 492, 389

Liller, M. H., & Liller, W. 1975, ApJ, 199, 133

Marscher, A. P. 2006, in Variability of Blazars II: Entering the GLAST Era, ed. H. R. Miller, K. Marshall, J. R. Webb, & M. F. Aller, ASP Conf. Ser., 350, 155

Marscher, A. P., et al. 2008, Nature, 452, 966

Marscher, A. P., Gear, W. K., & Travis, J. P. 1992, in Variability of Blazars, ed. E. Valtaoja & M. Valtonen (Cambridge U. Press), 85

Mattox, J. R., et al. 1996, ApJ, 461, 396

Schlegel, D. J., Finkbeiner, D. P., & Davis, M. 1998, ApJ, 500, 525

Spergel, D. N. et al. 2007, ApJS, 170, 377

Steffen, W., et al. 1995, A&A, 302, 335

Teräsranta, H., et al. 1998, A&AS, 132, 305

Vlahakis, N. 2006, in Blazar Variability Workshop II: Entering the GLAST Era, ed. H. R. Miller et al., ASP Conf. Ser., 350, 169

Vlahakis, N., & Königl, A. 2004, ApJ, 605,656

Williams, R. K. 2004, ApJ, 611, 952

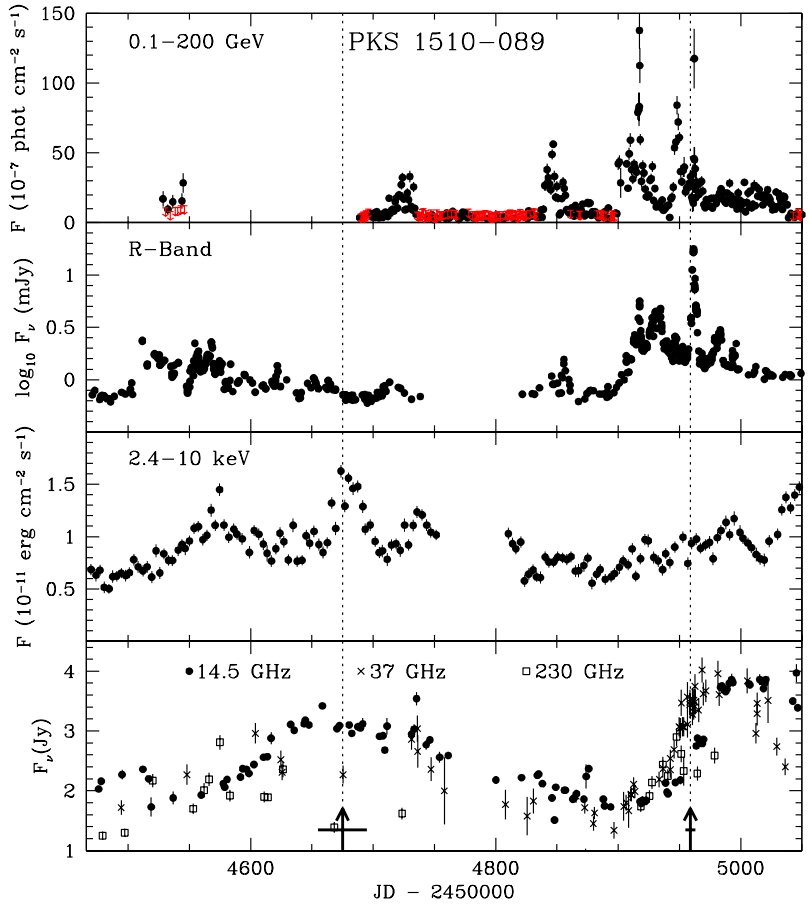

Fig. 1.— Multi-waveband light curves from 2008.0 to 2009.6. Upper limits (red) are 2-σ. R-band flux is uncorrected for reddening. Vertical arrows: times when superluminal knots passed the 43 GHz core; horizontal bars: uncertainties in these times. For reference, JD 2454700=2008 August 21, 2454900=2009 March 9.

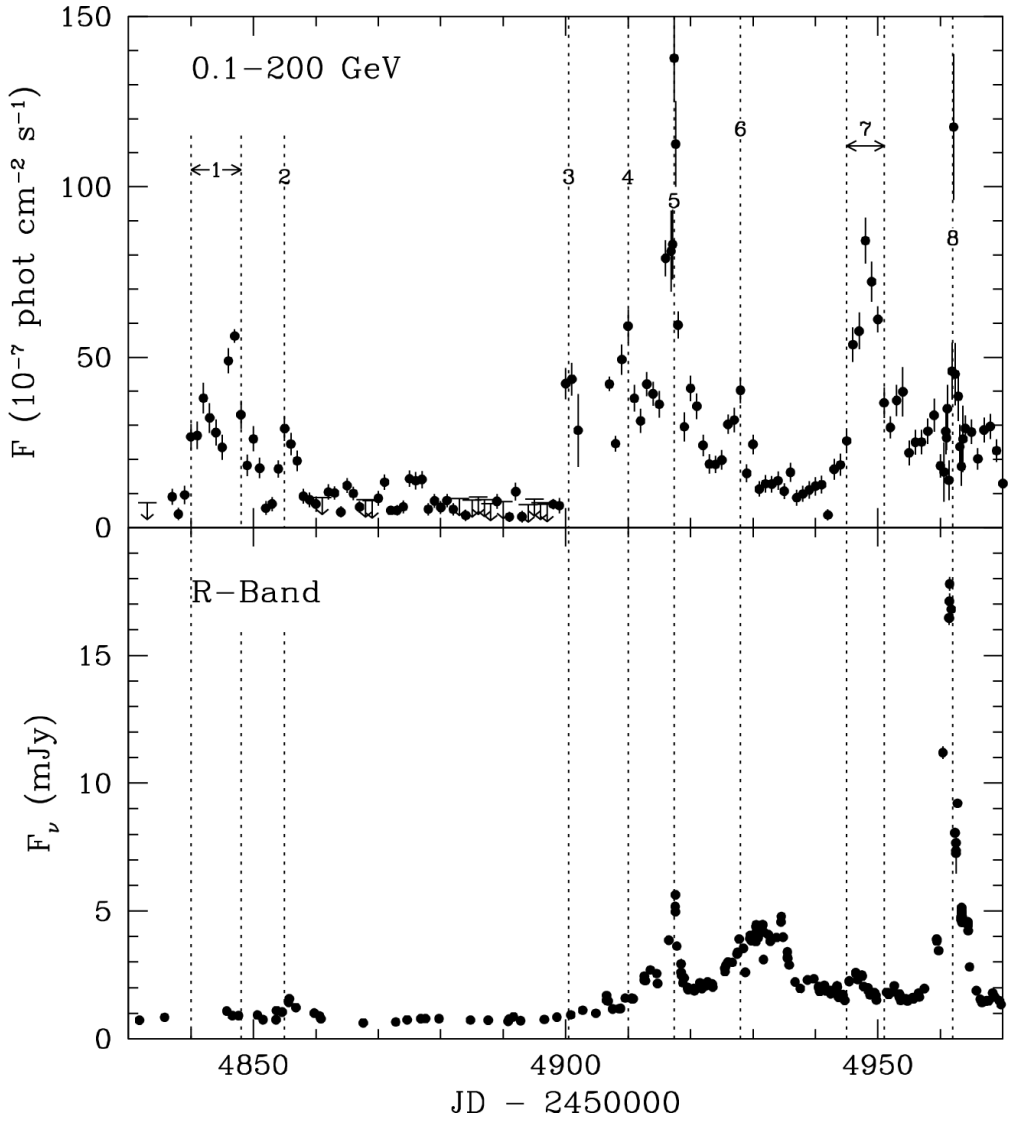

Fig. 2.— γ-ray and optical light curves from 2009.0 to 2009.38. See caption to Fig. 1. Vertical dotted lines denote γ-ray flares discussed in text.

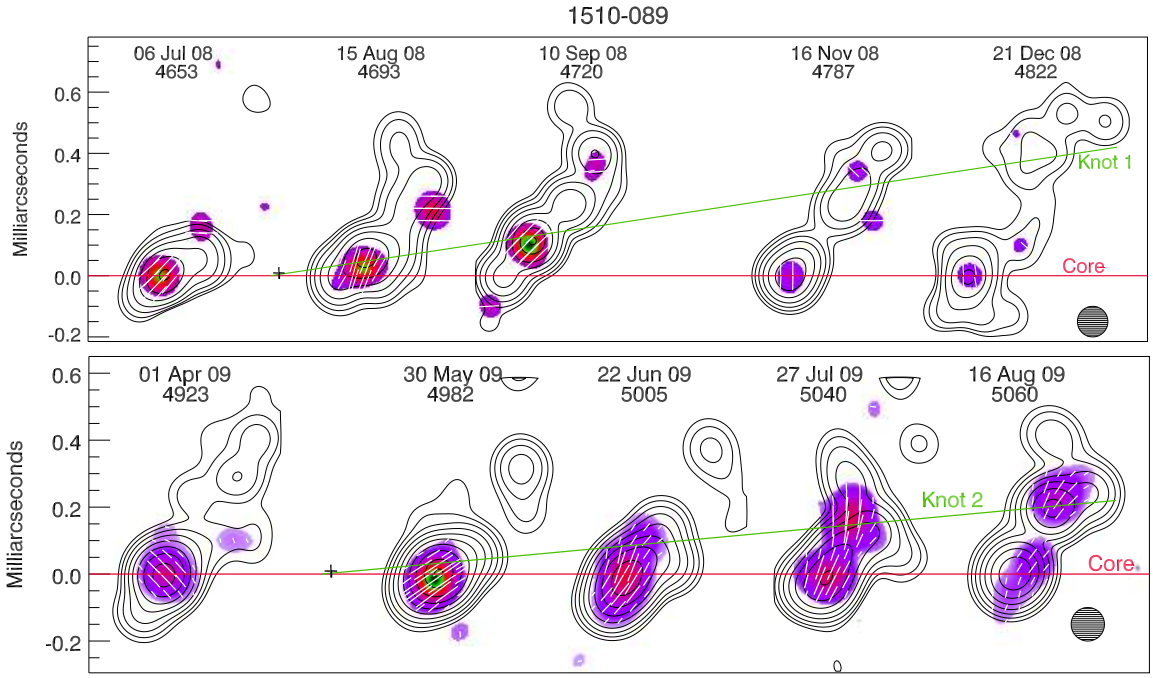

Fig. 3.— Sequence of 43 GHz VLBA images showing ejections of two superluminal knots with proper motions of (top) 1.1 ± 0.1, (bottom) 0.97 ± 0.06 mas yr^{-1}. Images are convolved with a circular Gaussian beam of FWHM=0.1 mas (shaded circle on bottom right). Calendar dates and JD−2450000 of images are given. Contours: total intensity, with levels (*top*) 1, 2, 4,..., 64, 96% of peak of 1.41 Jy beam^{-1}, and (*bottom*) 0.25, 0.5, 1, 2,..., 64, 96% of peak of 3.14 Jy beam^{-1}. White line segments: direction of linear polarization; color: polarized intensity relative to peak (green) of (*top*) 71 mJy beam^{-1} and (*bottom*) 120 mJy beam^{-1}. Polarization not correction for Faraday rotation, whose value is poorly constrained (Jorstad et al. 2007).

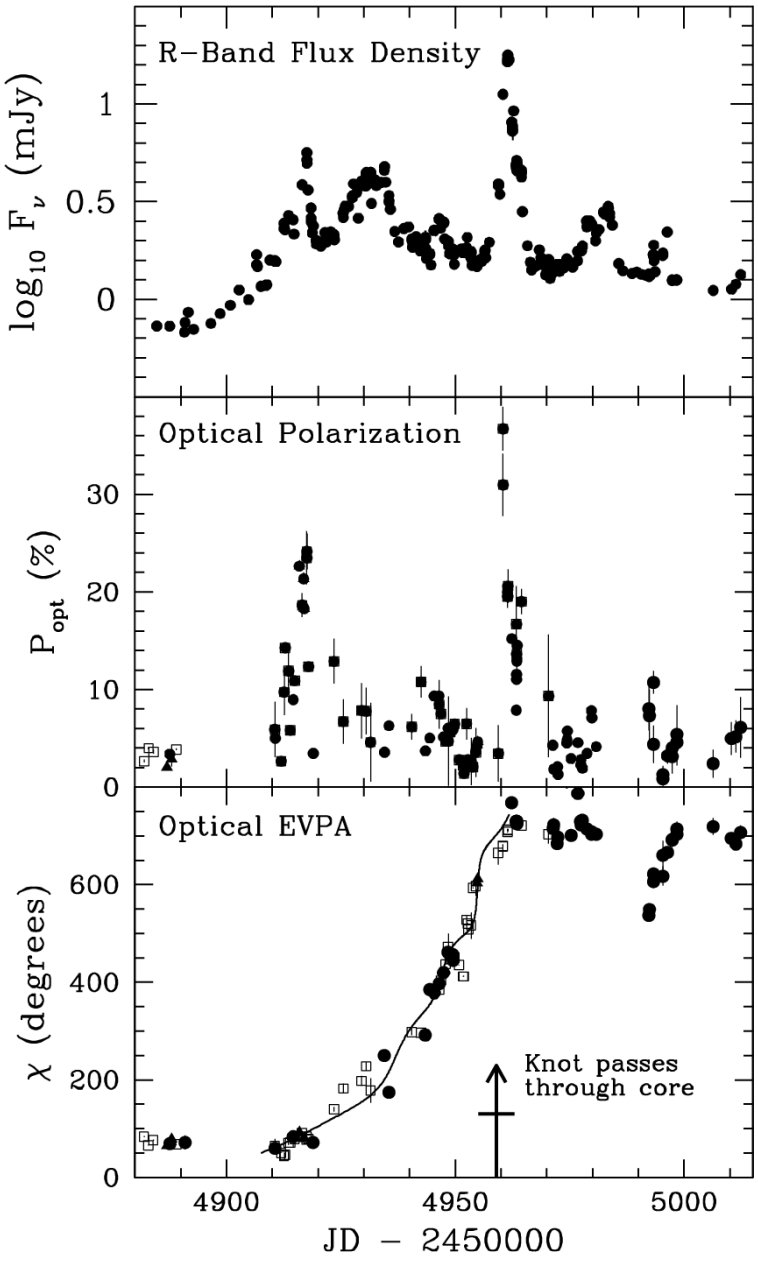

Fig. 4.— R-band flux density and degree P and electric-vector position angle χ of optical polarization in early 2009. Filled black circles: R-band; filled triangles: V-band; open squares: λ =500-700 nm. Multiples of 180° are added to χ as needed to minimize jumps in consecutive values of χ or, after JD 2454990, so the values of χ can be compared with the end of the first rotation. The curve fits the χ data with the model discussed in the text. Highest amplitude optical flare peaked on JD 2454962=2009 May 10.

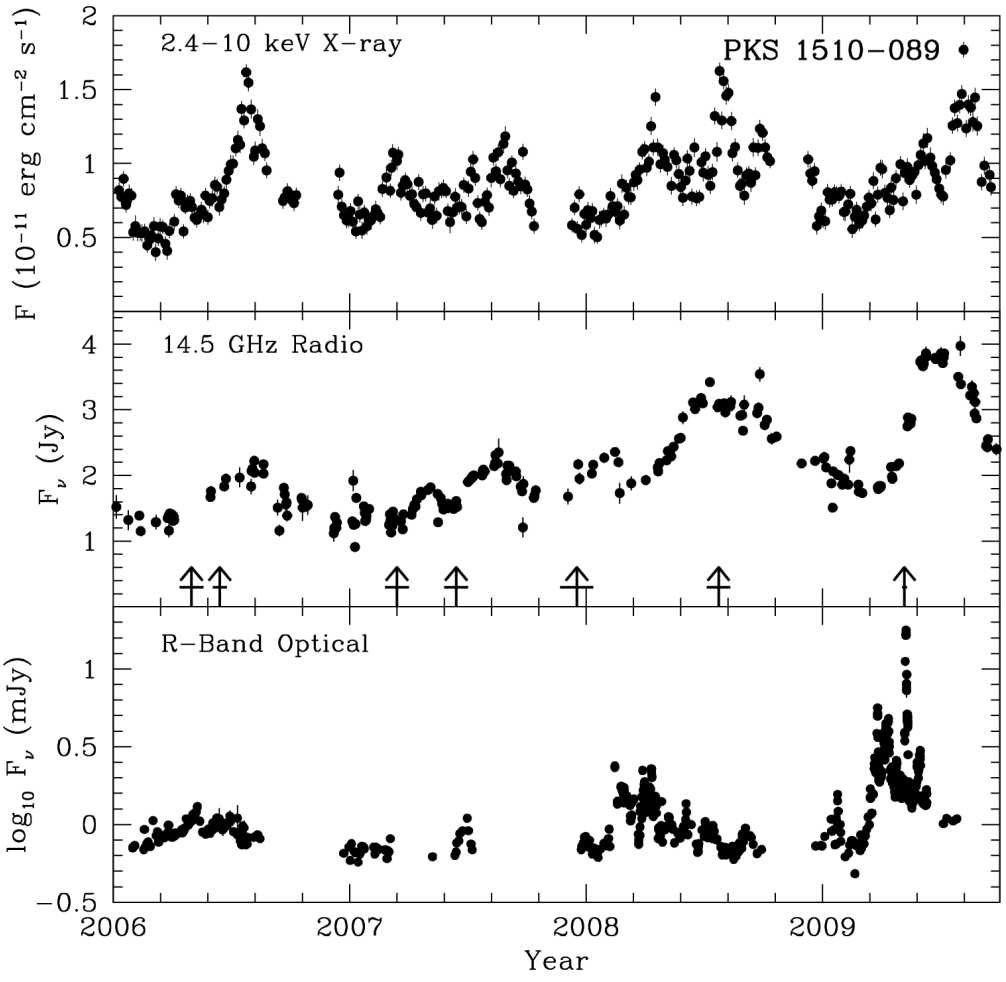

Fig. 5.— Variation of X-ray, radio, and optical flux of PKS 1510−089 from 2006.0 to 2009.7. See caption to Fig. 1.